Semi- Annual Status Report

MODELING OF TRANSIENT HEAT PIPE OPERATION

By
Gene T. Colwell
George W. Woodruff School of Mechanical Engineering
Atlanta, Georgia 30332

Submitted to
National Aeronautics and Space Administration
Langley Research Center
Hampton, Virginia 23665

NASA Technical Officer
Charles J. Camarda
Mail Stop 396

Under
NASA GRANT NAG-1-392

Period Covered
August 19, 1986 through February 18, 1987

JULY 1, 1987

GEORGIA INSTITUTE OF TECHNOLOGY
A UNIT OF THE UNIVERSITY SYSTEM OF GEORGIA
SCHOOL OF MECHANICAL ENGINEERING
ATLANTA, GEORGIA 30332

1987

MODELING OF TRANSIENT HEAT PIPE OPERATION

1. Introduction

The use of heat pipes is being considered as a means of reducing the peak temperature and large thermal gradients at the leading edges of reentry vehicles and hypersonic aircraft, and in nuclear reactors[1,2]. In the basic cooling concept, the heat pipe, which is a highly effective heat transport device, covers the leading edge, a portion of the lower wing surface, and a portion of the upper wing surface. Aerodynamic heat is mainly absorbed at the leading edge, and transported through the heat pipe to the upper and lower wing surface, where it is rejected by thermal radiation and convection. Once fully operational, the near isothermal heat pipe virtually eliminates temperature gradients and reduces peak temperatures.

A previous feasibility study[1] of heat pipes for this application recommends a rectangular cross-section for the heat pipe based on weight per unit surface area of heat pipe cooling structure and fabrication considerations. A schematic diagram of the physical model based on results presented in referenece[1] is shown in Figure 1.

Previous experimental observations[2-8] suggests the following sequence of events during heat pipe startup from the frozen state. Initially the working fluid is in the solid state and the vapor density is extremely low so that free molecular flow conditions prevail throughout the vapor space. The input heat flux over the evaporator starts to melt the frozen substance in this region, and the heat transport from the hot zone to the adjacent zone proceeds quite slowly via axial conduction through working fluid and capillary structure, and heat transfer in the vapor is almost negligible.

When energy is continuously added to the evaporator, the frozen working fluid in the evaporator is melted so that evaporation can take place at the liquid-vapor

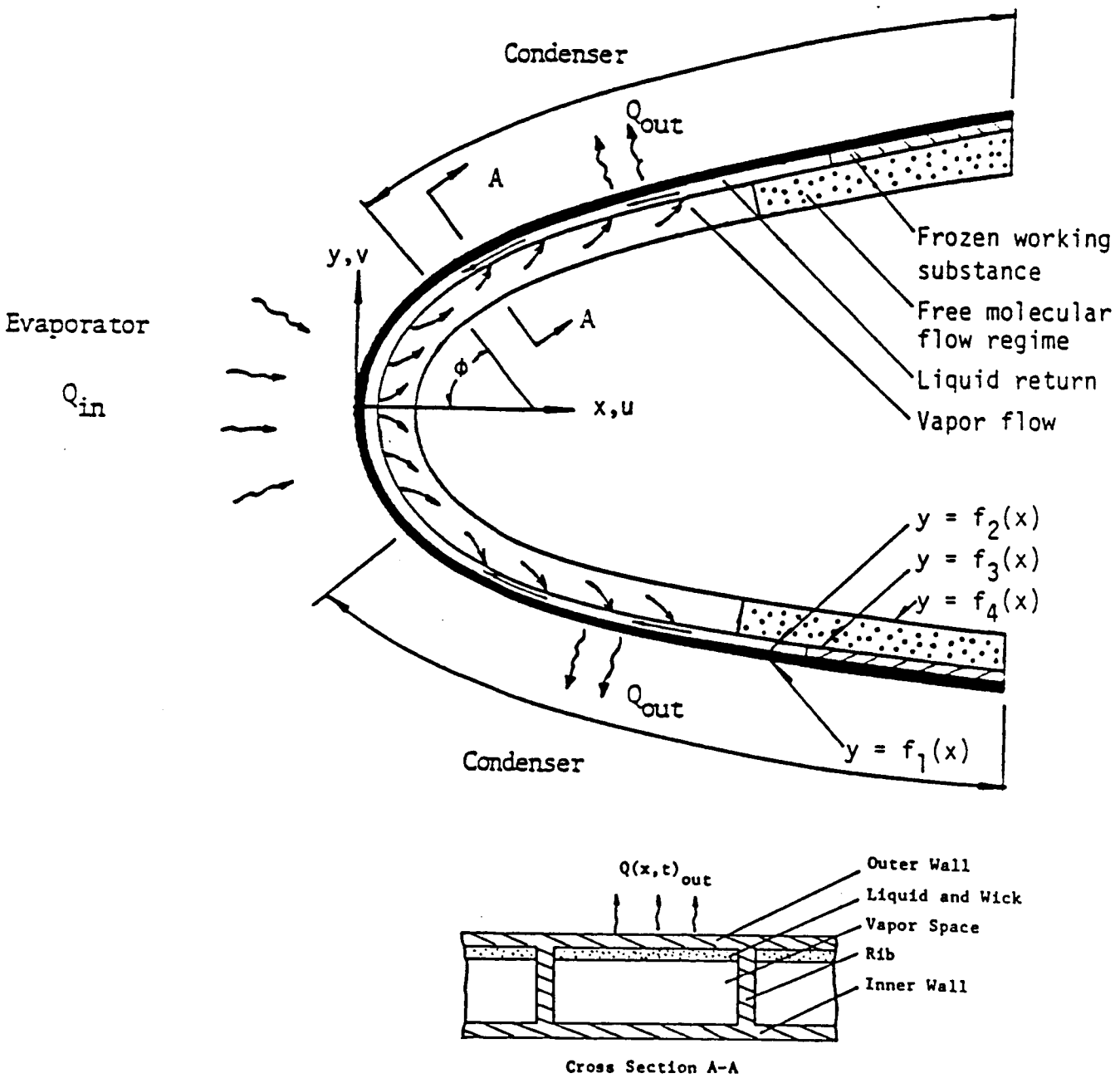

Figure 1. Schematic diagram of a heat pipe cooled leading edge.

interface and the vapor can flow into the condenser section due to the large pressure gradient. Hence, vapor freezes on the inner surface of the frozen working fluid in the cold zone so that the vapor-solid interface temperature increases until the melting temperature is reached. During this stage, energy is mainly transferred as latent heat owing to vaporization in the heated zone, and condensation and freezing in the cooled zone. Also, vapor flow may be choked at the exit of the evaporator because of very low pressure in the cold zone.

This process continues until the frozen working fluid is completely melted and the continuum flow regime reaches the end of the heat pipe, at which time liquid returned to the evaporator is sufficient for normal transient operation. Eventually the heat pipe may reach a steady state condition. As suggested, during the startup of the heat pipe from a frozen state, the behavior of vapor flow may be divided into three distinct phases for convience of analysis.

Phase I: The vapor flow in the heat pipe is in free molecular flow through the vapor space.

Phase II: In the vapor space, a region of continuum flow is established in the heated zone and a continuum flow front moves toward the heat pipe end. The vapor flow may be choked at the end of the evaporator.

Phase III: Continuum flow exists over the entire heat pipe length in the vapor region and the sonic limit is not encountered.

2. Mathematical Model Development

On the basis of experimental observations, basic governing equations are written to determine the startup, transient, and steady state performance of a heat pipe which has initially frozen alkali-metal as the working fluid. These equations can be coupled by several types of boundary conditions on the heat pipe surface, such

as specified temperature, heat flux, convection and radiation boundary conditions. The boundary condition at the liquid-vapor interface depends on the three phases of vapor flow dynamics mentioned in section 1.

2.1 Transition temperature

Continuum flow in the vapor space is considered to be established when the mean free path,λ, is substantially less than the minimum dimension,D, of the vapor flow passage, e.g.,

$$K_n \equiv \frac{\lambda}{D} \leq 0.01 \tag{1}$$

From kinetic theory of gases[9], the dynamic viscosity, and the mean molecular velocity can be expressed as

$$\mu = 0.499\rho\lambda V \tag{2}$$

$$V = \sqrt{\frac{8R_uT}{\pi M}} \tag{3}$$

Eliminating the mean free path from equations(2) and (3) yields the temperature of the vapor space corresponding to the given mean free path,

$$T^* \geq \frac{\pi}{2\times 10^{-4}} \frac{M}{R_u} \left(\frac{\mu}{\rho D}\right)^2 \tag{4}$$

where ρ is the density of the vapor, μ is the dynamic viscosity of the vapor, R_u is the universal gas constant, and M is the molecule weight.

Iterations are required to obtain a value of T* due to the dependence of temperature of properities. Figure 2 illustrates the transition temperature, T*, from free

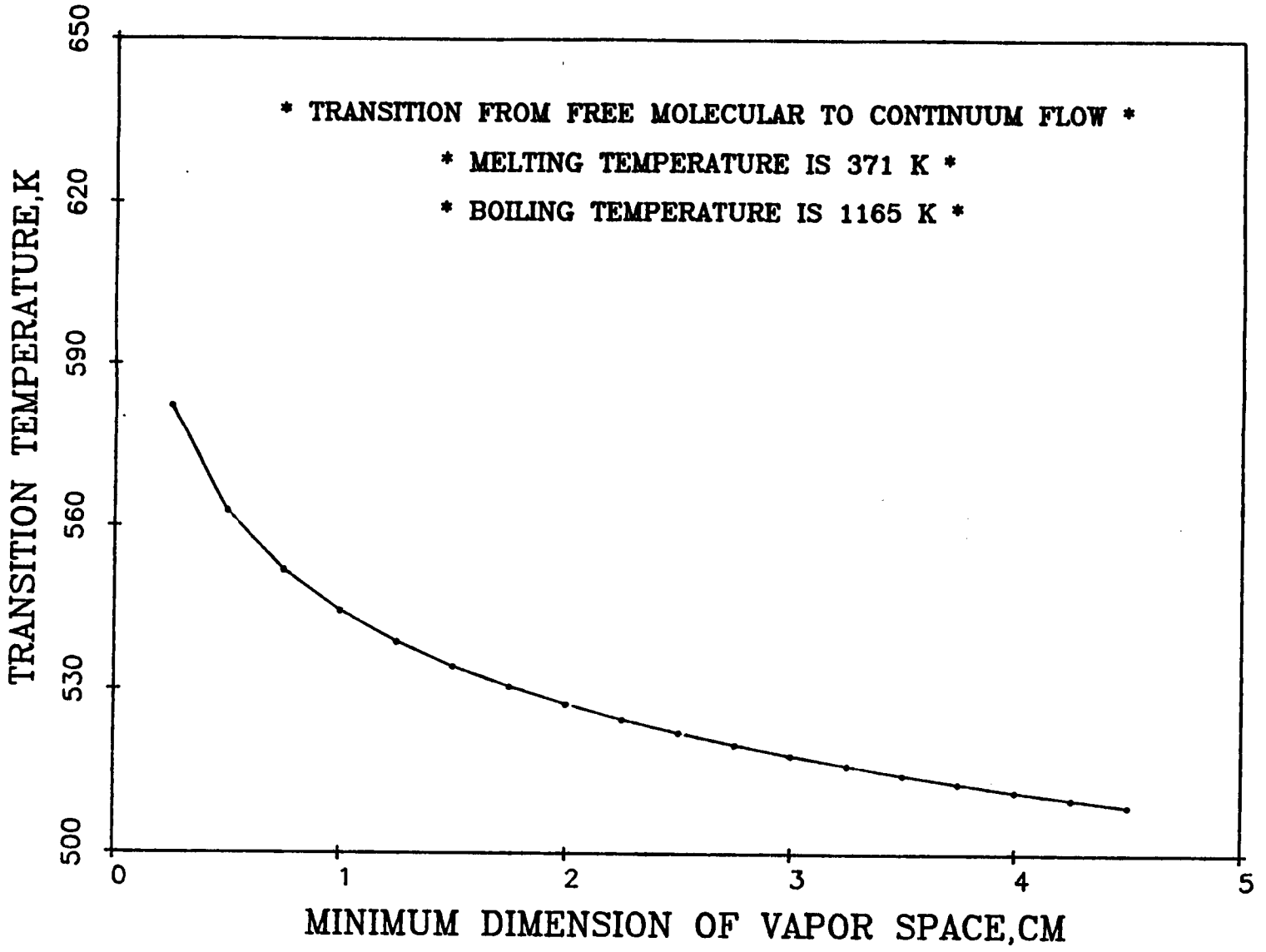

Figure 2. Transition temperature for sodium as heat pipe working fluid.

molecular to continuum flow as a function of minimum vapor passage for sodium. When the temperature of the vapor space is greater than that calculated by Equation(4), continuum flow is assumed to be established in the vapor space.

2.2 Heat pipe shell and capillary structure with fluid

Unlike those for a conventional cylindrical heat pipe, aerodynamic heating will cause the highest temperature to occur at the outer shell of heat pipe. Thus, to simplify the analysis, it is assumed that the inner shell is sufficiently thin to neglect its thermal resistance and capacitance. Furthermore, the following additional assumptions are made. The thickness of the heat pipe and the rib is assumed to be much smaller, than the width, and temperature gradients would be developed primarily in the chordwise direction during heat pipe startup. Therefore, the rib may be neglected in the analysis. Also, the heat pipe is assumed to be symmetric about the stagnation line so that the upper half section of the heat pipe is considered. Hence, a two-dimensional model is considered for mathematical formulation, and a simplified cross section is shown in Figure 3.

The unsteady, two-dimensional conduction equation is applied to the heat pipe shell and the capillary structure to evaluate the temperature distributions under the following assumptions:

1. The heat transfered through the wick and working fluid is by conduction only;
2. The presence of the wick structure does not affect the melting of the working substance, and melting occurs over a small, finite temperature range, ΔT, around the melting temperature;
3. The boundary conditions at the liquid-vapor interface are subject to the phases of vapor flow dynamics noted in section 1.

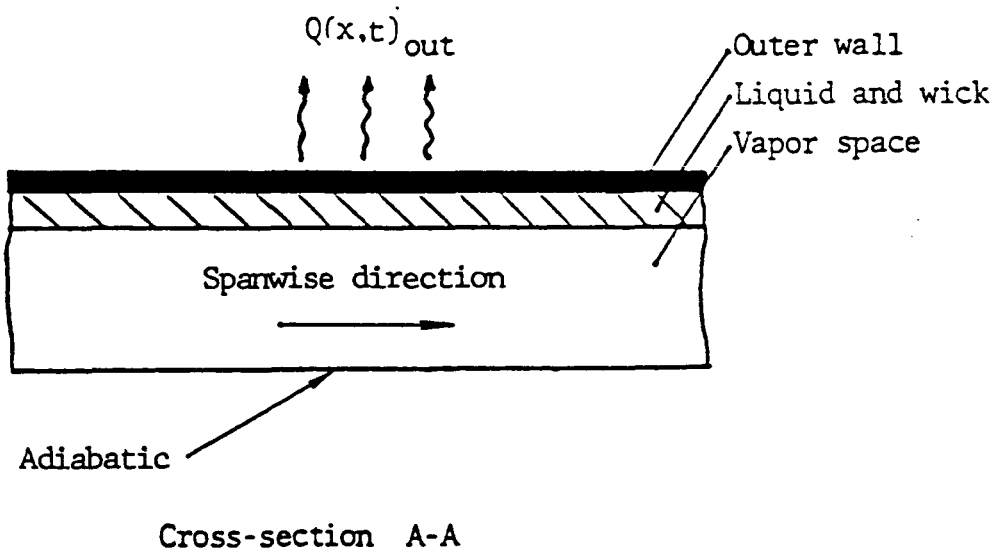

Figure 3. Simplified cross-section A–A of the heat pipe cooled leading edge.

4. The radiation heat transfer at the liquid-vapor interface is neglected based on the small thermal emissivity of liquid sodium measured[10].

The governing equations and boundary conditions for the heat pipe shell and capillary structure with working fluid are expressed in the same form:

$$C_i \frac{\partial T_i}{\partial t} = \frac{\partial}{\partial X}\left(K_i \frac{\partial T_i}{\partial X}\right) + \frac{\partial}{\partial Y}\left(K_i \frac{\partial T_i}{\partial Y}\right) \quad , \quad i = 1,2 \tag{5}$$

$$T_i = T_\circ \qquad \text{for t} < 0 \tag{6}$$

$$-K_1 \frac{\partial T_1}{\partial t} = \ddot{Q}(X,t) \quad \text{at} \quad Y = f_1(X) \quad \text{for} \quad 0 \le \psi \le \psi_e \tag{7}$$

$$-K_1 \frac{\partial T_1}{\partial t} = h_{cr}(T_1 - T_{cr}) + \sigma\varepsilon({T_1}^4 - {T_r}^4) \quad \text{at} \quad Y = f_1(X) \quad \text{for} \quad \psi_e \le \psi \le \psi_c \tag{8}$$

$$T_1 = T_2 \quad \text{and} \quad K_1 \frac{\partial T_1}{\partial n} = K_2 \frac{\partial T_2}{\partial n} \quad \text{at} \quad Y = f_2(X) \quad \text{for} \quad 0 \le \psi \le \psi_c \tag{9}$$

$$\frac{\partial T_i}{\partial S} = 0 \qquad \text{at} \qquad \psi = 0 \quad \text{and} \quad \psi = \psi_c \tag{10}$$

where the subscripts 1 and 2 denote the heat pipe shell and the capillary structure, n represents the unit outward normal direction, and S represents the chordwise direction.

In the X - Y coordinates

$$K\frac{\partial T}{\partial n} = K\frac{\partial T}{\partial X}l_x + K\frac{\partial T}{\partial Y}l_y \tag{11}$$

where l_x and l_y are the direction cosines between the surface outward normal, n, and the X, and Y axes, respectively.

2.3 Analysis of the vapor flow

Analysis of the vapor flow is necessary to provide the boundary condition at the liquid-vapor interface when continuum flow is established in part of the vapor space. However, the behavior of the vapor flow as mentioned in section 1 is very complicated due to the extremely small vapor density of the metallic working fluid at low vapor pressure and the large pressure gradient in the axial direction. Limits on the vapor flow are encountered and considerable thermal resistance exists at the liquid-vapor interface due to phase change of the working fluid. The case of a flat plate heat pipe with asymmetrical boundary conditions shown in Figure 3 is considered for the vapor flow passage.

Evaporation and condensation

From kinetic theory, a significant thermal resistance exists at the liquid-vapor interface for liquid metal[11] and this resistance increases with decreasing vapor pressure. This means that the difference between the vapor temperature and the interface temperature is not negligible. At the interface, the interphase mass transfer has been stated from the viewpoint of kinetic theory as a net molecular flux which is the difference between the rate of arrival of molecules from the vapor space towards the interface and vice-versa. While condensation is proceeding, the arrival rate of molecules exceeds the departure rate. During evaporation, the reverse takes place,

and during the equilibrium state, a net molecular flux is zero. Hence, evaporation and condensation are modeled by using an expression for the net rate derived from the kinetic theory of gases[12]:

$$\dot{m}_\circ = \left(\frac{2a}{2-a}\right)\sqrt{\frac{M}{2\pi R_u}}\left[\frac{P_f}{\sqrt{T_f}} - \frac{P_v}{\sqrt{T_v}}\right] \tag{12}$$

where a is the condensation or evaporation coefficient which is assumed to be unity, $\dot{m}_\circ$ is the rate of condensation or evaporation per unit area, M is the molecular weight,R_u is the universal gas constant, P_f and T_f are pressure and temperature, respectively, at the interface, and P_v and T_v are pressure and temperature of vapor, respectively.

Limitations of vapor flow

After continuum flow is established in the vapor space, because of the low density of vapor at low pressure and the large pressure gradient, the vapor flow is choked at the end of the evaporator, even for a low heat flux, just as it is at the throat of a convergent nozzle. This sonic limit is the first amoung several limitations encountered, and the performance of the heat pipe is restricted until the vapor temperature increases significantly so that the velocity of the vapor leaving the evaporator is less than the sonic velocity.

The expression for the sonic limit[6,13] in terms of flow conditions at the beginning of the evaporator by energy balance on a control volume enclosing the entire evaporator is:

$$Q_s = \frac{\rho_\circ A h_{fg}\sqrt{\gamma R_u T_\circ}}{\sqrt{2(\gamma+1)M}} \tag{13}$$

where A is the cross-section area of vapor space, h_{fg} is the enthalpy of vaporization, γ is the ratio of specific heat, M is the weight of a molecule,R_u is the universal gas

constant, T_o is the vapor temperature the beginning of the evaporator and γ_o is taken as the saturation density corresponding to T_o. Experimental verification of Equation(13) has been made by Kemme[14] for sodium, potassium and cesium heat pipes.

Figure 4 shows the sonic limit, the entrainment limit[15] and the Reynolds Number for a heat pipe which has a cross-section area of 0.55 cm^2, hydraulic radius of .32 cm, 100 mesh screen wick, and sodium as the working fluid. The type of limitation restricting performance of heat pipe is determined by which limitation has the lowest value at the temperature under consideration. Thus, the first limit encountered is the sonic limit, as shown in Figure 4. However, when the actual axial heat transfer required is below these limits, no limits are encountered.

Modeling of vapor flow during phase II

Even though some of the working substance is in the liquid state, the transition temperature from free molecular flow to continuum flow is much greater than the melting temperature, so the vapor is assumed to be free molecular during phase I, and an adiabatic boundary condition is applicable at the interface. However, during phase II, a region of continuum flow is assumed to be established in the adjacent vapor space when the interface temperature is greater than the transition temperature, while in the cold zone the vapor is still in free molecular flow. The continuum flow region grows until it reaches the end of the heat pipe. The temperature in the region of free molecular flow remains unchanged except in the vicinity of the continuum flow region. Therefore, an imaginary plane, which is adiabatic and normal to the liquid-vapor interface, is assumed to divide the two vapor flow regions at the point of the transition temperature, and the dividing plane moves toward the end of the heat pipe as the location of the transition temperature at the interface moves.

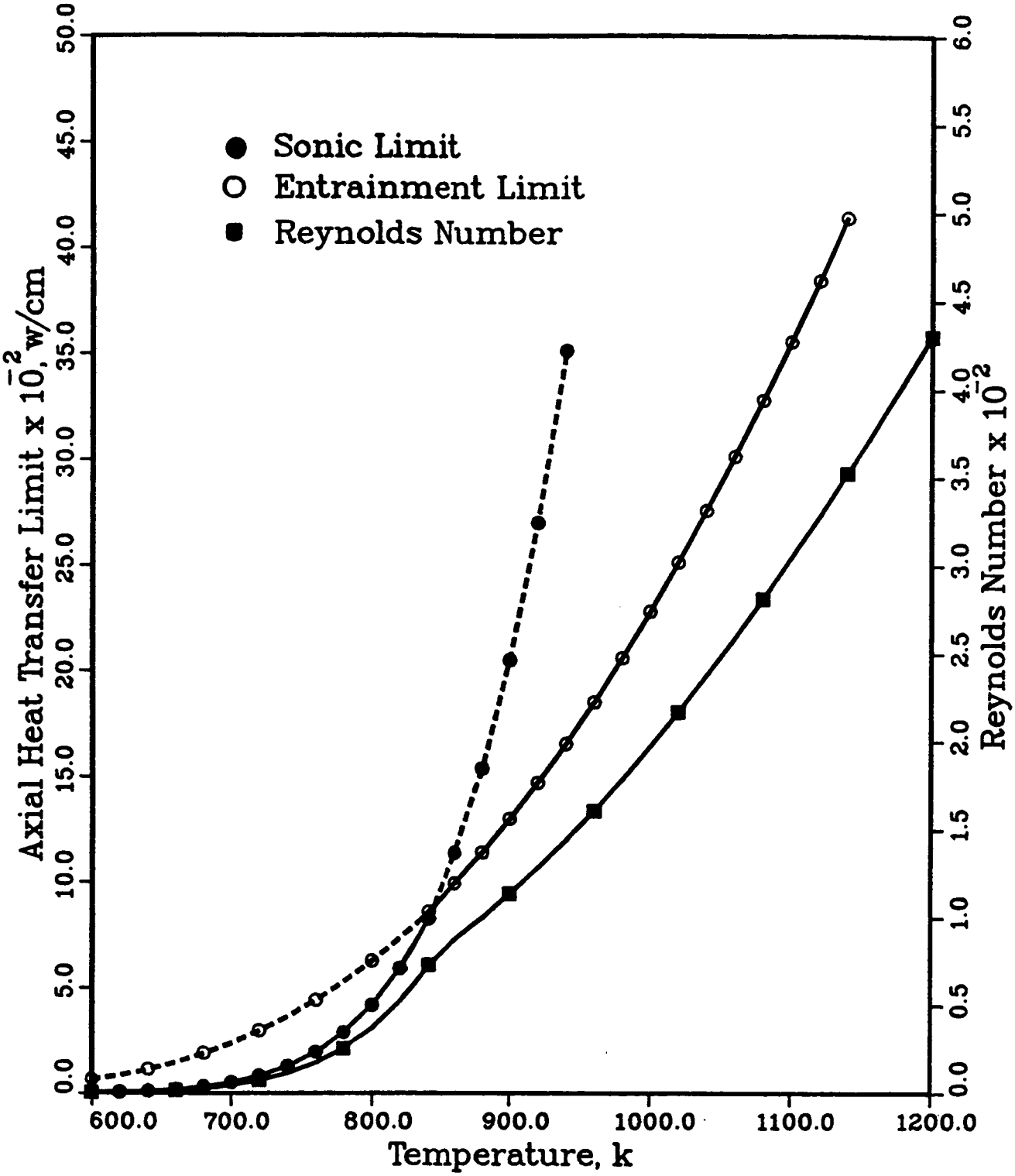

Figure 4. Heat pipe vapor flow limits and correspondinf Reynolds Number.

In the continuum flow region, energy is mainly transported as latent heat of the working fluid, and variations of temperature and pressure in the axial direction are significant. Even though continuum flow exists in the vapor space, the vapor pressure is low and the pressure gradient in the axial direction is large, so the heat transfer is limited by the choked flow condition, and supersonic vapor flow and a shock front[6,7,16] may occur in the condenser.

In this research, the overall performance of a heat pipe is of more interest than the details of one portion, and as noted, the ultimate heat transfer rate in the axial direction is limited by the sonic limit. Thus, the vapor flow during phase II may be approximated without loosing the generality and accuracy by evaluating the sonic limit properly. In order to evaluate the sonic limit, the total heat input to the vapor space, which can be obtained by applying Equation(12) to the element adjacent to the continuum flow region, is equated to the sonic limited transport from Equation(13) as follows:

$$\sum_{i=1}^{m} \sqrt{\frac{M}{2\pi R_u}} \left[\frac{P_{f_i}}{\sqrt{T_{f_i}}} - \frac{P_v}{\sqrt{T_v}} \right] W = \frac{\rho A_c \sqrt{\gamma R_u T_v}}{\sqrt{2(\gamma+1)M}} \tag{14}$$

where A_c is the cross-section area and W is the width of the vapor space. From Equation(14), the uniform vapor temperature can be computed by iteration. This vapor temperature may be lower than true vapor temperature at the beginning of the evaporator, but at this stage the variation of density with temperature and the density itself is very small, so the variation of sonic limit with respect to temperature is also small, as shown in Figure 4. Thus, the heat flux at the liquid-vapor interface and the sonic limit can be obtained by solving Equations(12) and (13), respectively, with the vapor temperature obtained from Equation(14). This method may be used until the vapor flow state reaches phase III.

Vapor flow during phase III

In this stage, the entire working fluid is completely melted and continuum flow exists throughout the vapor space. However, the heat pipe has not reached the desired operating condition and the density of the vapor is still small, so that compressibility should be considered. Also the amount of energy stored in the vapor space is negligible. Thus, quasi-steady, compressible, one-dimensional laminar flow in the vapor space is considered. For purposes of formulating the mass, momentum, and energy equations in one-dimensional form, the velocity is taken to be the average velocity, which is approximated by the velocity distributions based on the similarly solutions of semiporous channels. In addition, friction at the liquid-vapor interface, variations of vapor quality, and momentum and energy factors are similarly calculated. The vapor is evaporated at the interface with mass injection rate,$\dot{m}_\circ$, per unit area. It is assumed that this vapor flows inward with a normal component of velocity only, and joins the axial flowing stream.

The principles of conservation of mass, momentum, and energy in the axial direction, and the assumptions noted, yield:

$$D\frac{d}{dZ}(\rho V) = \dot{m}_\circ \tag{15}$$

$$\frac{dP}{dZ} + \frac{d}{dZ}(\alpha\rho V^2) = -\frac{F\rho V^2}{8D} \tag{16}$$

$$D\frac{d}{dZ}\left[\rho V(h_v + \frac{\beta V^2}{2})\right] = \dot{m}_\circ(h_\circ + V_\circ{}^2) \tag{17}$$

where D is the height of the vapor space, h_v is the vapor enthalpy and $h_\circ$ is the vapor enthalpy at the interface.

Friction factor F of the surface is written as

$$F = \frac{8\tau_v}{\rho V^2} \tag{18}$$

Momentum and energy factor, α and β, respectively, are expressed as

$$\alpha = \frac{1}{DV^2}\int_0^D U^2 dy \tag{19}$$

$$\beta = \frac{1}{DV^3}\int_0^D U^3 dy \tag{20}$$

Normal velocity of the vapor at the interface is expressed in terms of heat flux and latent heat of vaporization as follows:

$$V_0 = \frac{\dot{Q}}{h_{fg}\rho_\circ A_\circ} \tag{21}$$

where $\dot{Q}$ is the heat input rate at the interface, $\rho_\circ$ is the density for the interface temperature and $A_\circ$ is the interface area.

Coupling vapor flow effects

When the Mach number is less than about 0.2, compressibility is neglected and friction effects at the interface may be negligible due to the low velocity of the vapor. Thus, most studies[17,18] of heat pipe performance have assumed that the temperature is uniform throughout the vapor space. This approximation eliminates difficulties encountered from solving the vapor flow dynamics and gives simple results for the case of a low operating temperature with the small heat flux. When the vapor temperature is uniform in the vapor space, no thermal resistance exists, so a maximum amount of energy can be transfered through the vapor space for the given operating condition.

The energy stored in the vapor space is negligible due to low density, so the energy entering the evaporator is equal to the that leaving the condenser. Then Equation(12), which describes evaporation and condensation, is applied to every element at the interface, and the energy balance in the vapor space is:

$$\sum_{i=1}^{m_e}\left[\frac{P_{f_i}}{\sqrt{T_{f_i}}}-\frac{P_v}{\sqrt{T_v}}\right]=\sum_{i=1}^{m_c}\left[\frac{P_{f_i}}{\sqrt{T_{f_i}}}-\frac{P_v}{\sqrt{T_v}}\right] \tag{22}$$

where m_e is the number of elements at the interface in the evaporator and m_c is the number of elements in the condenser. Equation(22) can be solved by using iterations to obtain uniform vapor temperature as long as the temperature at the interface is known. Also, the heat flux at the interface is evaluated using Equation(12) with known temperatures.

However, when liquid metal is used as the working fluid and the heat flux applied to the surface is large, the velocity of the vapor is large, so the temperature drop in the vapor space should be considered. For a heat pipe which has a rectangular cross-section area of 1.77 cm^2, Figure 5 shows considerable temperature drops for large heat fluxes. The temperature drops in the vapor region imply that the thermal resistance causes less energy to be transferred from the evaporator to the condenser. Thus, the evaporator temperature is higher and the temperature of condenser is lower than in the other case.

When the vapor flow dynamics are coupled with the heat conduction in the heat pipe shell and capillary structure at the interface, the governing equations are solved simultaneously with unknown boundary conditions at the interface, so iterations are required for every time step until both results match at the interface. This method may yield accurate results, but in general consumes much computational time due to the iterations. Also convergence may not be reached. Hence, an approximation

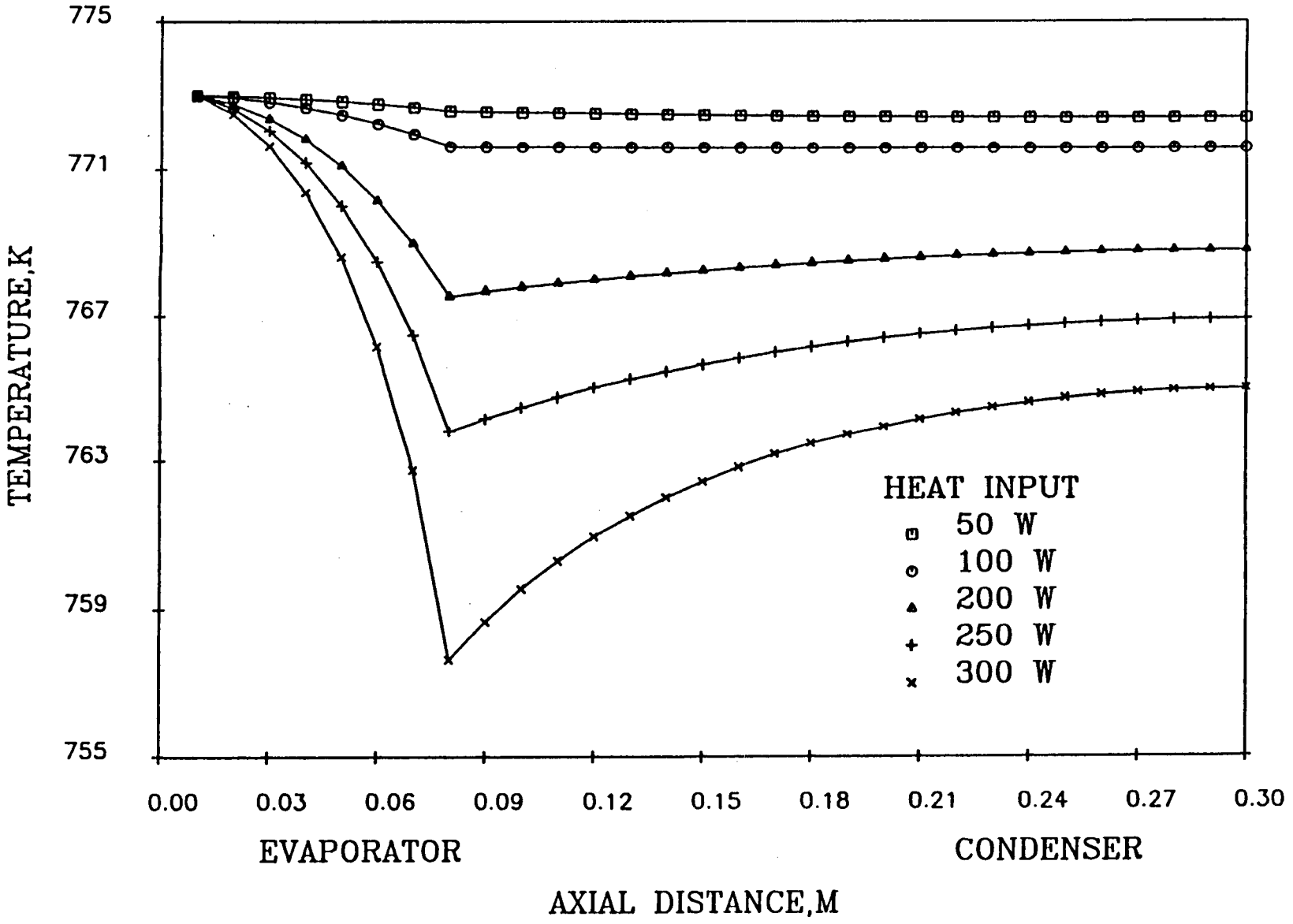

Figure 5. Axial variations of vapor temperature for various heat inputs.

method is employed to eliminate these difficulties.

Instead of simultaneously solving governing equations for both regions, governing equations for the vapor region are separately solved with given a heat flux, so that the temperature drop,$\triangle T_v$, can be obtained. The thermal resistance,R_v, in the vapor space may then be evaluated from Equation(22):

$$Q = \frac{\triangle T_v}{R_v} \tag{23}$$

In order to get thermal resistance, the total heat flow rate is needed, but without solving both governing equations, the heat flow rate is also unknown. Thus, the known heat flow rate at previous time step is used, and heat flow rate evaluated at the present time step would be used at the next time step.

When this evaluated thermal resistance is imposed at a different place without changing total heat transfer rate, the uniform vapor temperature can be used in the vapor space. Since the total heat transfer rate through the vapor space, which is computed by using Equation(12), is the same as the heat input at the liquid-vapor interface in the evaporator or heat output at the interface in condenser, a certain fictitious layer which has the same thermal resistance as that evaluated in the vapor space may be placed at the liquid-vapor interface. Thus, the temperature at the new interface is lower than that at the true interface due to the resistance in the fictitious layer for the evaporator, and vice-versa for the condenser.

In order to compute the uniform vapor temperature, the temperatures at the new interface are used for T_{f_i} in Equation(22), and the heat flux at the interface is calculated by using Equation(12) with the uniform vapor temperature and the temperatures at the new interfaces. This heat flux then serves as the boundary condition at the liquid-vapor interface when solving the governing equations for the

heat pipe shell, capillary structure, and vapor flow at the next time step. By using this approximation scheme, iterations can be excluded while the vapor flow effects are retained.

3. Results and Discussion

To verify the model developed for heat pipe cooled leading edges, numerical results are compared to Camarda's experimental results[2]. Since the shape of the cross-section of Camarda's model is different from that of the present model, the rectangular cross-section for this research is modeled such that the cross-section areas occupied by the heat pipe shell, the capillary structure, and the vapor space are the same as for his experiment. Also, the surface area where the heat flux is applied is chosen identical to that of the experiment so that the width and length of heat pipe are identical, but the thickness of the component between the two heat pipes is different. However, the thickness is much smaller than other dimensions, and the temperature drop at the cross-section is negligibly small compared to the temperature drop in the axial direction, so the effects of the difference in the thicknesses may be minimal. Thus, effects of energy storage and fusion of working fluid in the heat pipe shell and the capillary structure are the same, and the effect of vapor flow dynamics may be simulated. Since the minimum dimension of the vapor space is different due to a different thickness of the heat pipe, the transition temperature which is evaluated based on the dimension of the vapor space is not identical. Also, this temperature determines the boundary condition at the liquid-vapor interface, so to simulate the Camarda case, the inner diameter of the circular heat pipe is used to calculate the transition temperature.

The material of each component used in the computation is the same as in the experiment except that the Braze alloy is assumed to be hastelloy x to simplify the

heat pipe shell. The properities of the materials are varied with temperature during numerical calculation.

Heating distribution on the heat pipe surface is modeled based on the normalized heating distribution[2] shown in Figure 6, and time stepped heat input at the stagnation point. The stepped heating distribution due to aerodynamic heating is shown in Figue 7. In addition to aerodynamic heating, a radiation boundary condition is used to extract energy from the entire heat pipe surface so that the net rate affects heat pipe internal operation. The section which has a positive net rate is considered the evaporator, and the section with a the negative net rate is the condenser.

Figure 8 shows the two-dimensional grid system, dimensions, boundary conditions, and materials used to represent a leading edge cooling heat pipe. It is assumed that the temperature of the heat pipe is initially the ambient temperature, which is below the melting point of the sodium working fluid. Also, a transition temperature of 700 °K is used.

An explicit method with a few implicit steps is used as the time stepping scheme. Until continuum flow is established in the vapor space, a constant time step of 10 seconds is used. This time step is gradually decreased due to increasing the stepped heat input on the external surface.

Figure 9 shows a comparision of the numerical and experimental results along the heat pipe for different times. Detailed numerical results are plotted on Figures 10 and 11. Since most of the energy, which is transferred by conduction through heat pipe shell and capillary structure in the axial direction, is added near the stagnation point, the temperature near the stagnation point increases rapidly, and a large temperature gradient is established in the heat pipe. This implies that the heat pipe is not effective due to the extremely small vapor density up to about 550

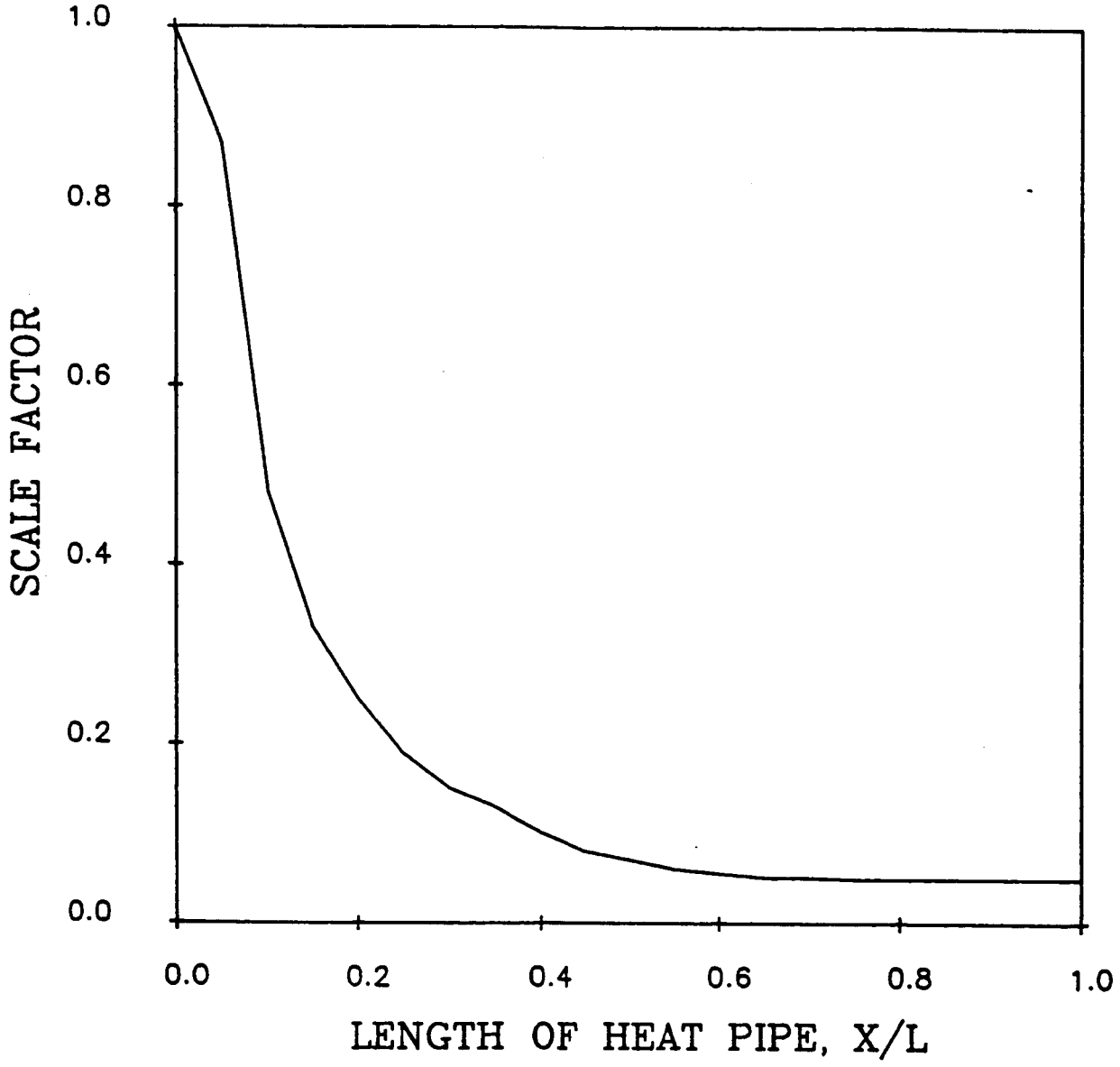

Figure 6. Normalized heating distribution

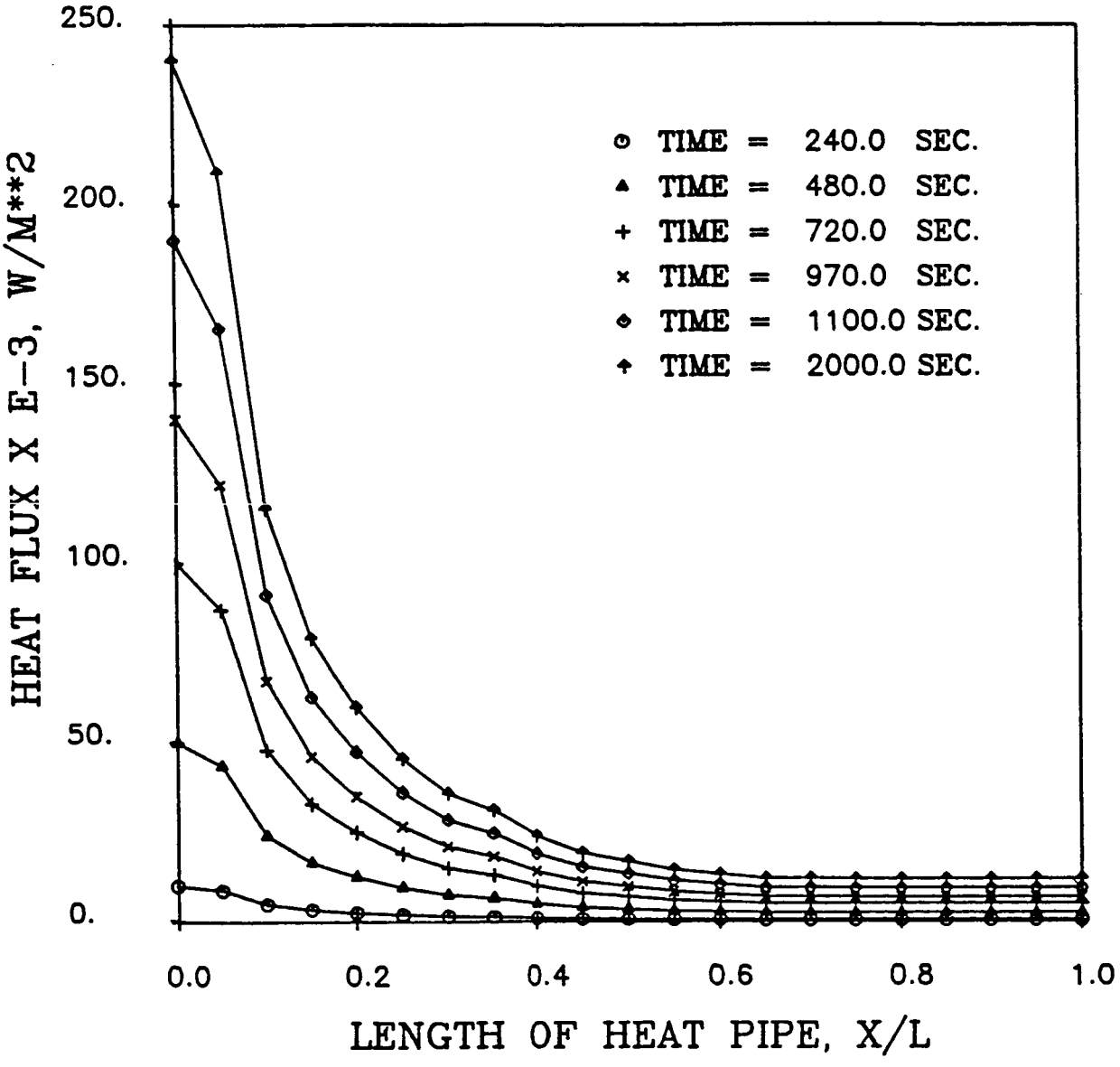

Figure 7. Heat flux distribution on a leading edge model

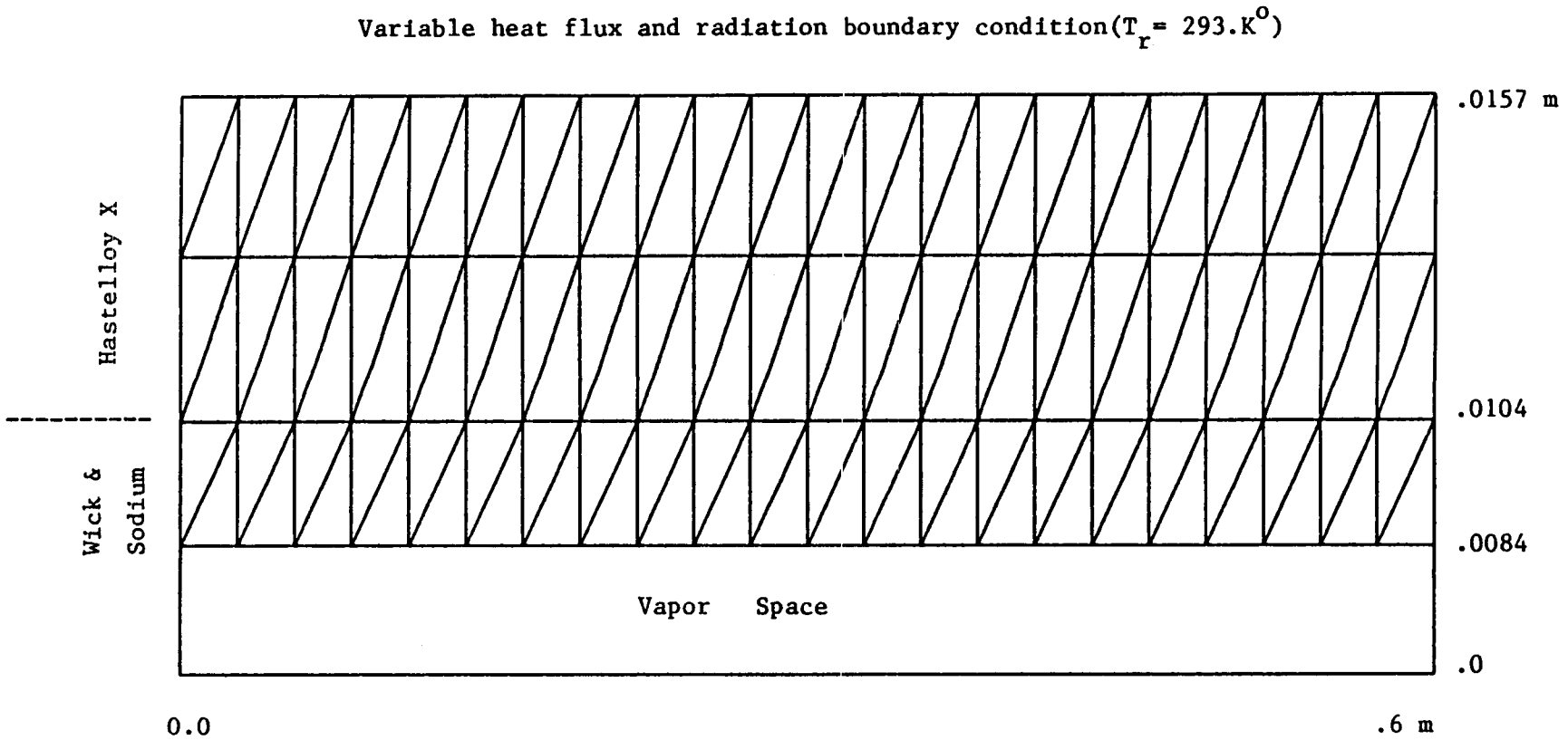

Figure 8. Two-dimensional mesh used to represent a leading edge cooling heat pipe; 138 elements, 96 nodes.

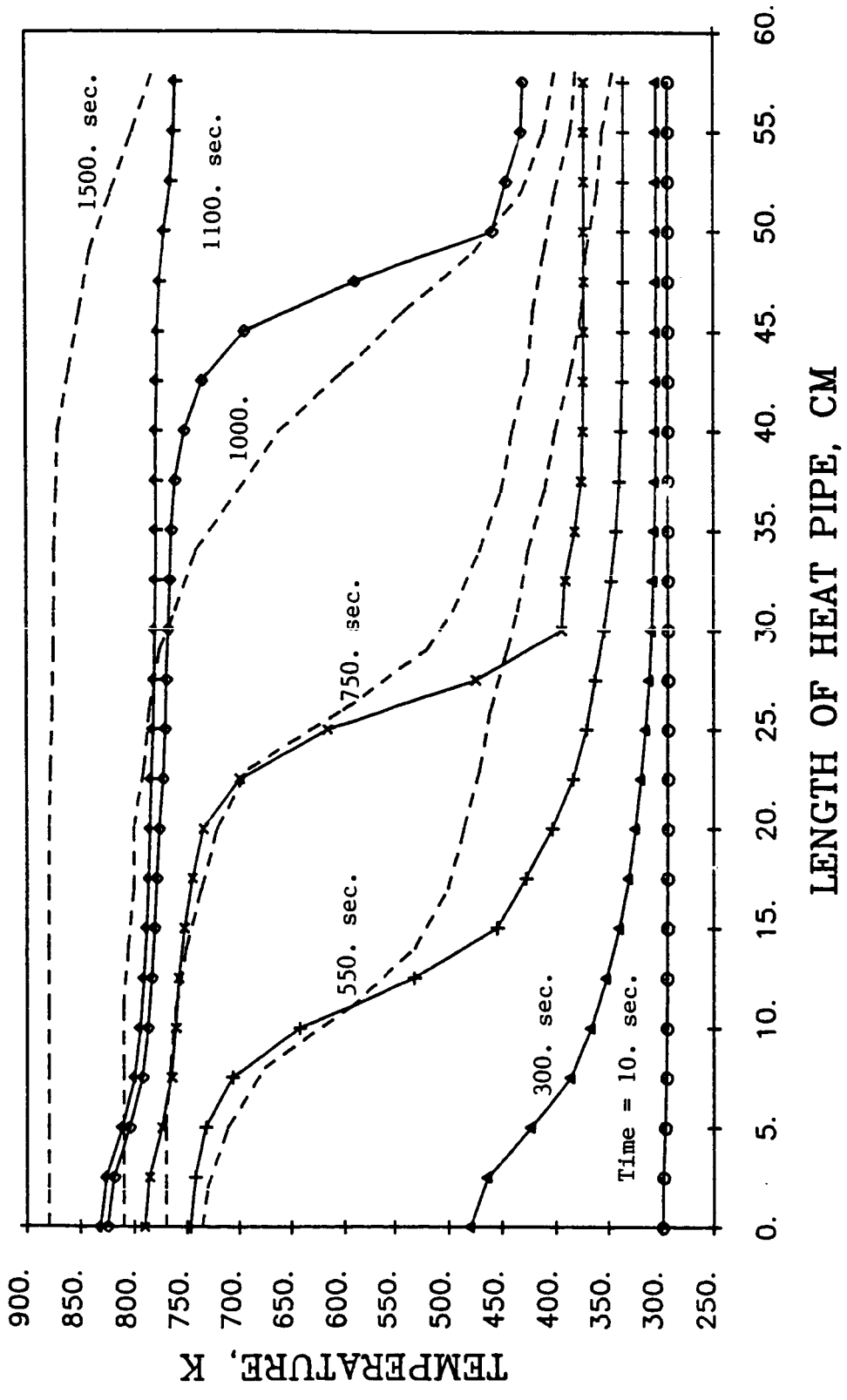

Figure 9. Temperature of a leading edge cooling heat pipe.

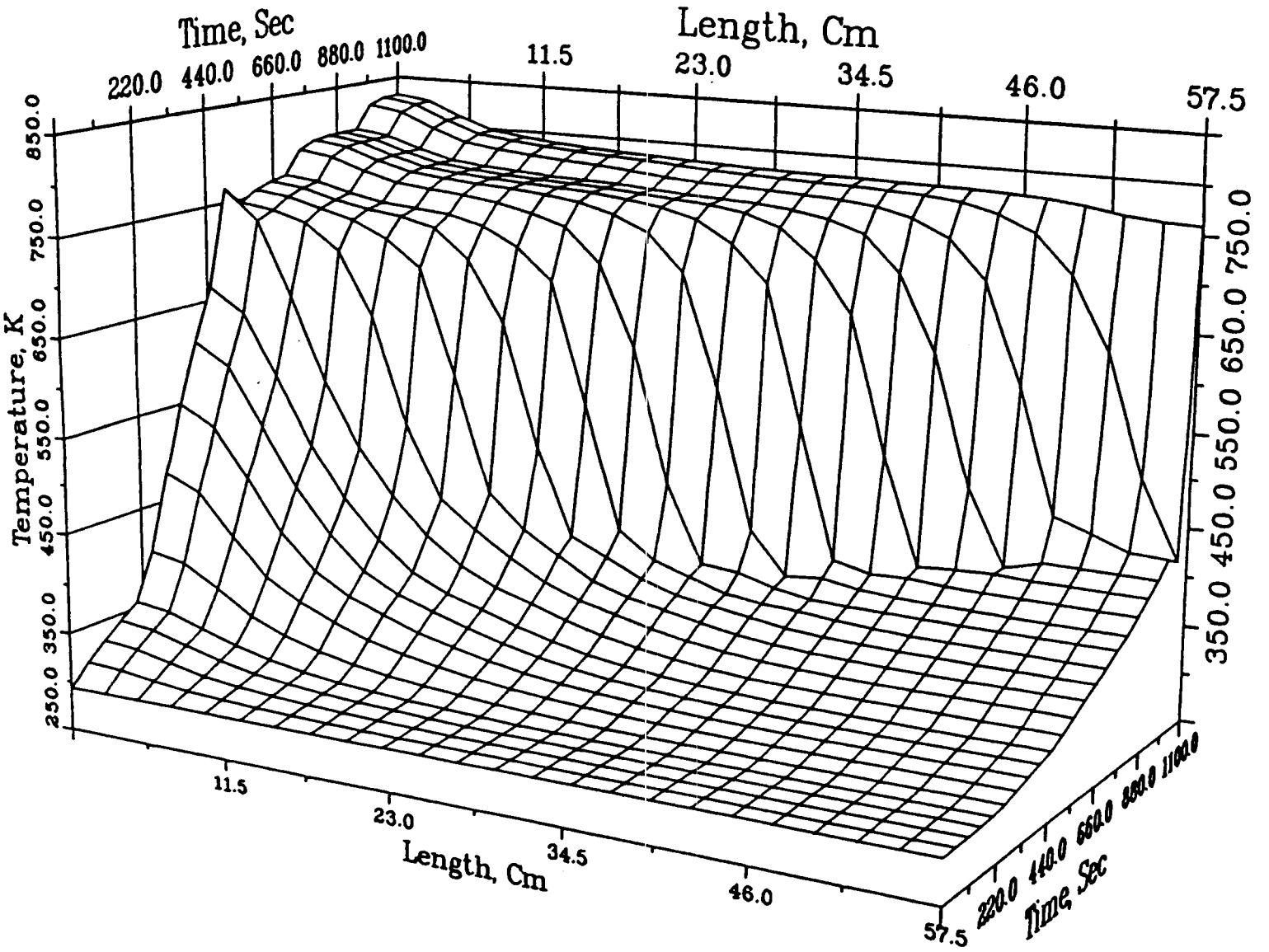

Figure 10. Temperature distributions at the surface.

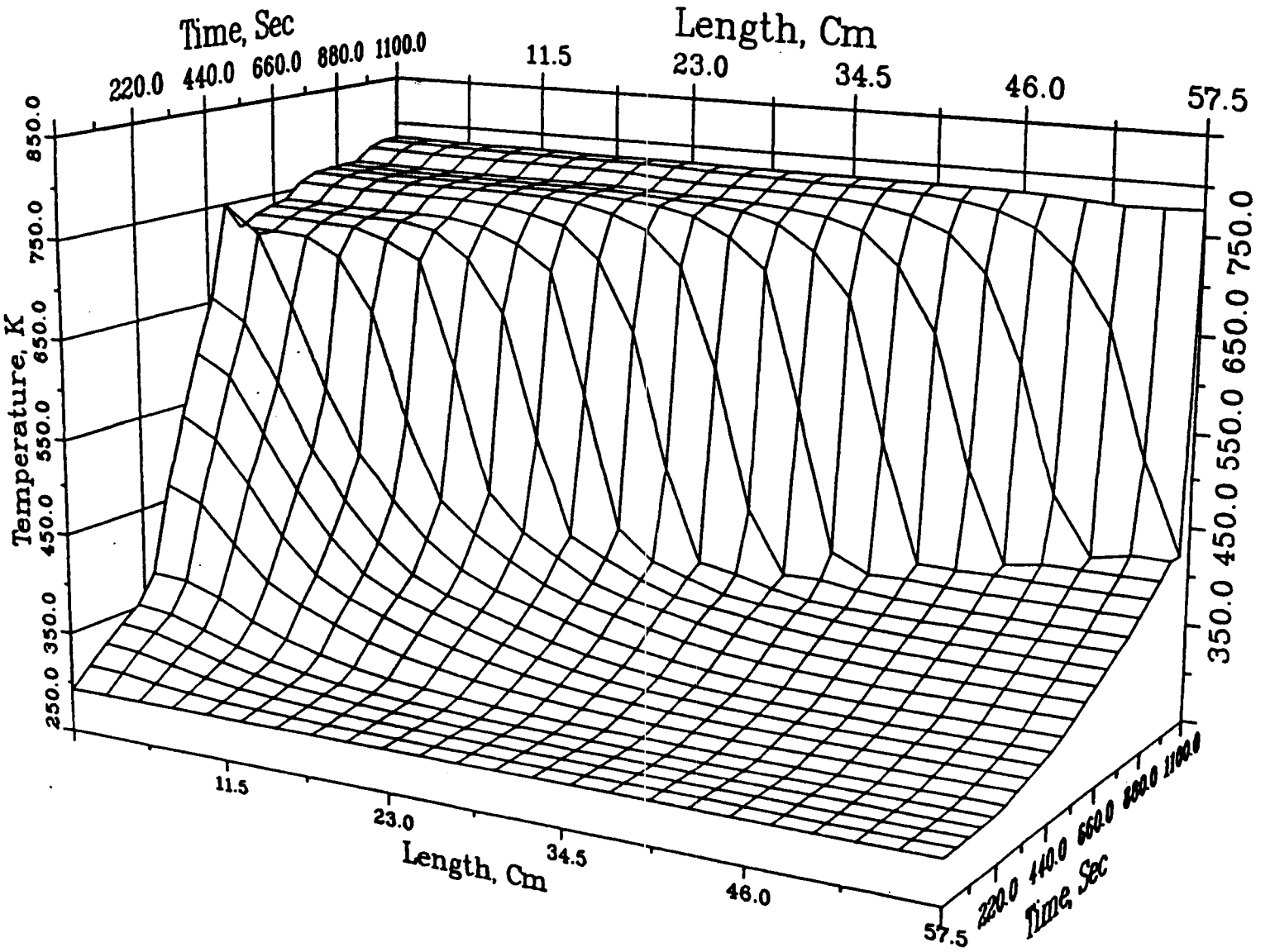

Figure 11. Temperature distributions at the interface.

seconds. Temperatures in the rest of the heat pipe are not much different from the initial condition. At 550 seconds, the temperature at the stagnation point is greater than the transition temperature, and temperature gradient at the region adjacent to this point decreases. This means that a continuum flow region is established in the vapor space, so energy is mainly transported by the latent heat. However, most of the working fluid is in the frozen state and free molecule flow prevails in the vapor space. As time increases, the continuum flow region is expanded in the vapor space so that at about 750 seconds one-third of the heat pipe performs as a heat pipe. The rest of the heat pipe is still like a solid in which heat is transported only by conduction. Between the two regions, a large temperature gradient exists, and the continuum flow front is located here. At 1000 seconds, most of the heat pipe is active except near the end of the condenser section, and the working fluid is completely melted. After 1500 seconds, the heat pipe reaches a fully operational condition.

Figures 10 and 11 show temperature distributions at the external surface and the interface, respectively, obtained by numerical analysis. Figure 12 shows the vapor temperature variation during startup. The vapor temperature increases corresponding to increasing heat flux. However, the vapor temperature increases very slowly because most of the heat added in the vapor space of the evaporator is extracted at the interface of the condenser to heat up the adjacent cold zone.

Even though the numerical results do not match exactly the experimental results due to different configuration, material properties and boundary conditions, it is clear that the model does predict approximately the correct startup-time and approximately the correct temperature distribution. It is important to note that heat inputs to the model were based on aerodynamic heating computation which were only approximated in the experiments.

Finally, to show the effectiveness of the heat pipe for cooling a leading edge, numerical calculations were executed for the same example problem, except that an adiabatic boundary condition was applied to the interface during the entire startup. Development of large axial temperature gradients is identical due to the free molecular condition in the entire vapor space in the first part of transient heating. However, beyond this stage, peak temperatures are reduced and temperature gradients disappear when the heat pipe is active. Figure 13 shows temperature distributions for both cases at a time of 1100 seconds. It is clear that the heat pipe is very effective in reducing temperature near the leading edge.

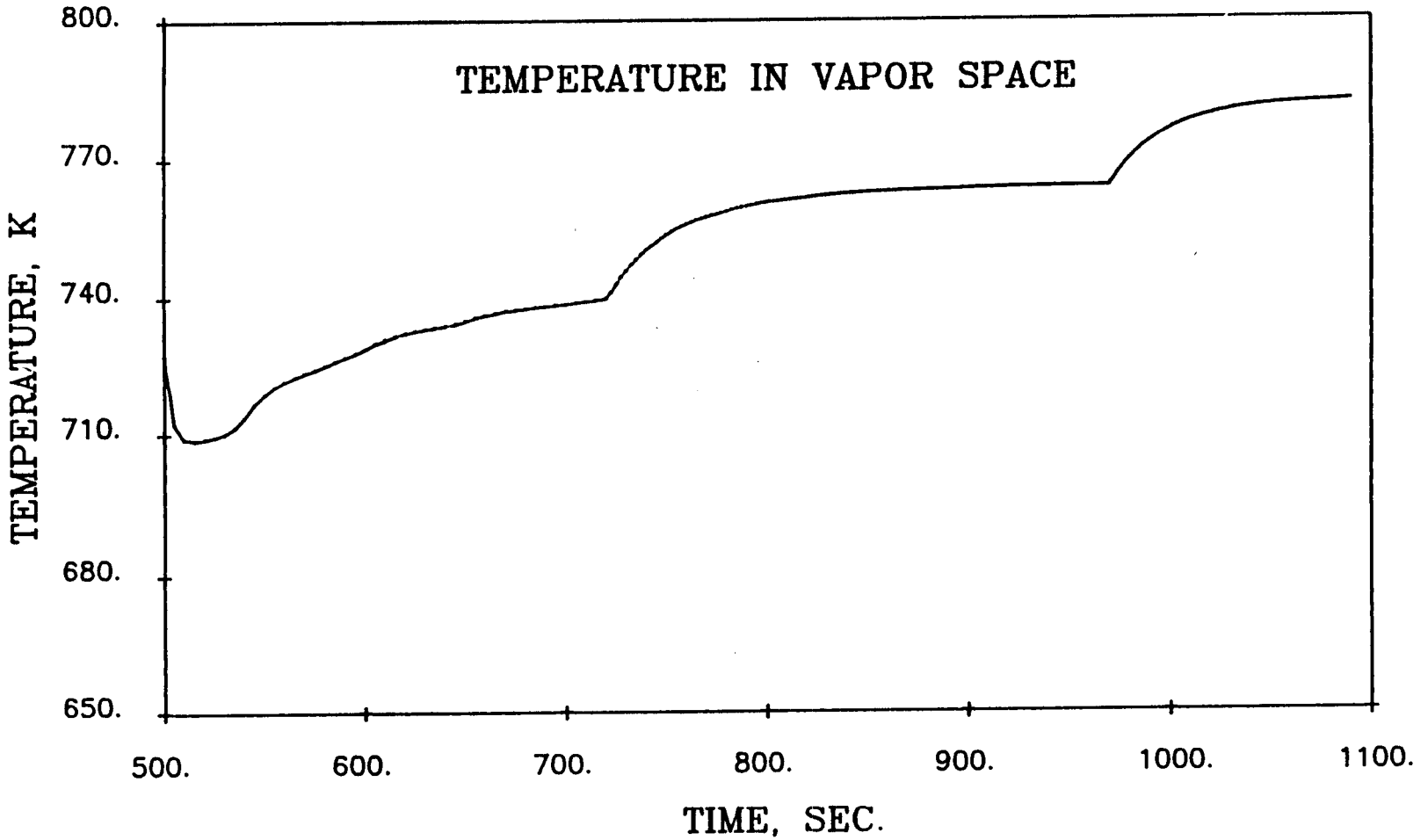

Figure 12. Vapor temperature variation during startup.

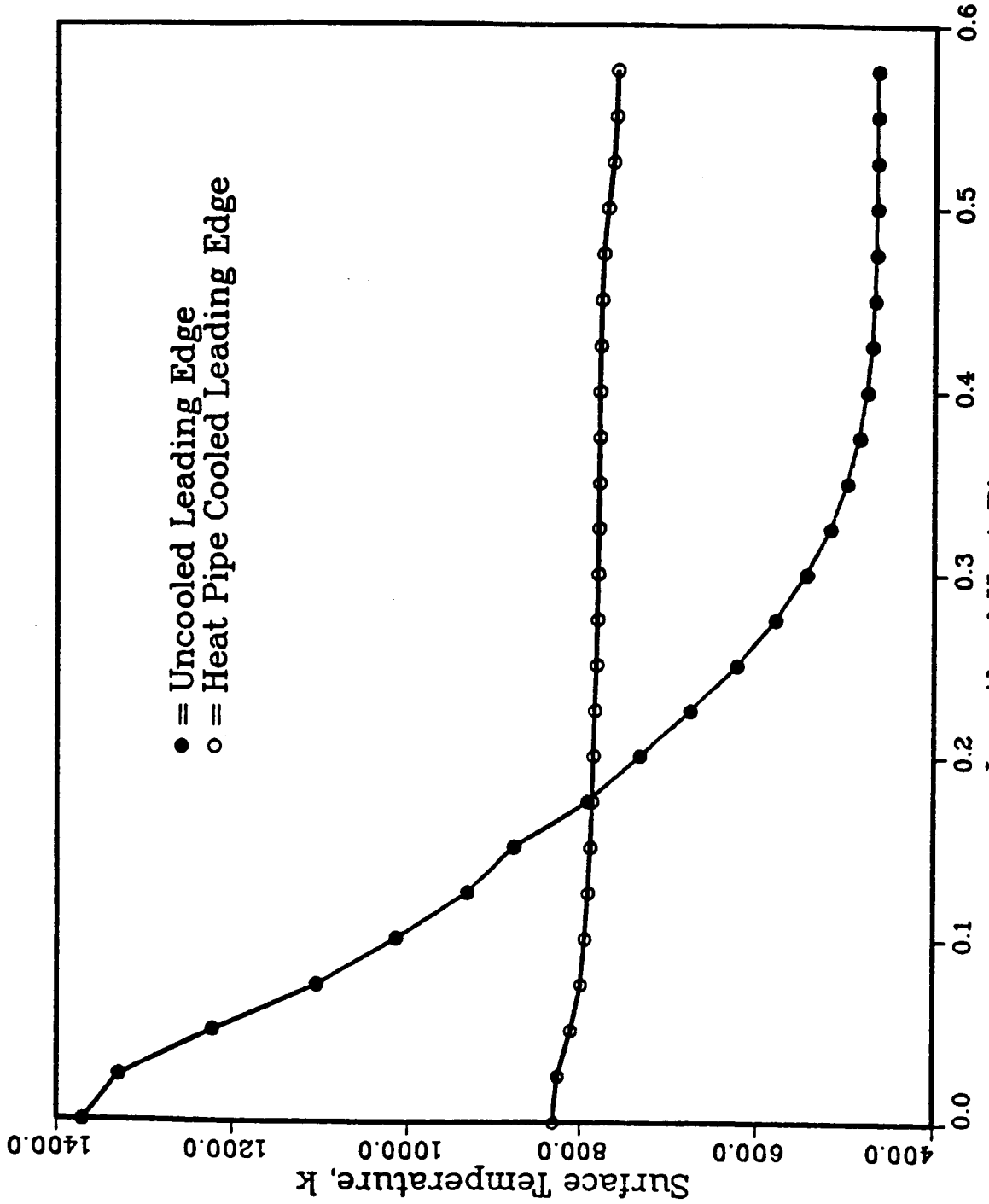

Figure 13. Computed temperature distributions for uncooled and cooled leading edge; t = 1100 sec.

REFERENCES

1. C. C. Silverstein, "A Feasibility Study of Heat-Pipe-Cooled leading Edges for Hypersonic Cruise Aircraft," NASA CR - 1857, Nov. 1971.

2. C. J. Camarda, "Analysis and Radiant Heating Tests of a Heat-Pipe-Cooled Leading Edge," NASA TN - 8486, Aug. 1977.

3. T. P. Cotter, "Heat Pipe Startup Dynamics," Proc. IEEE Thermionic Conversion Specialist Conference, Palo Alto, Calif, Oct. 1967.

4. L. G. Neal, "An Analytical and Experimental Study of Heat Pipes," TRW Systems, Jan. 1967.

5. A. P. Shlosinger, "Heat Pipe Devices for Space Suit Temperature Control," TRW System Rept. No. 06462 - 6005 -RO-00, Nov. 1968.

6. J. E. Deverall, J. E. Kemme, and L. W. Florschuetz, "Sonic Limitations and Startup Problems of Heat Pipes," LA - 4518, 1970.

7. M. N. Ivanovskii, V. P. Sorokin, and I. V. Yagodkin, " The Physical Principles of Heat Pipe," Clarender Press, Oxford, 1982.

8. M. A. Merrigan, E. S. Keddy, and J. T. Sena, "Transient Heat Pipe Investigations for Space Power Systems," LA - UR - 05 -334I, 1985.

9. E. R. G. Eckert and R. M. Drake, "Analysis of Heat and Mass Transfer," McGraw - Hill Book Co., New York, 1972.

10. N. Hattori, "Emissivity of Liquid Sodium," Heat Transfer Japanese Research, Vol. 13, No. 1, 1984, PP. 30 - 40.

11. S. P. Sukhatme and W. M. Rohsenow, "Heat Transfer During Film Condensation of a Liquid Metal Vapor," J. of Heat Transfer, Feb. 1966, PP. 19 - 28.

12. J. G. Collier, "Convective Boiling and Condensation," McGraw - Hill Book Co., New York, 1981.

13. E. K. Levy, "Theoretical Investigation of Heat Pipes," Proc. Aviation and Space Conference, Beverly Hills, Calif., 1968.

14. J. E. Kemme, "Ultimate Heat-Pipe Performance," IEEE Trans. Electron Devices, Vol. ED - 16, No. 8, Aug. 1969.

15. S. W. Chi, "Heat Pipe Theory and Practice," McGraw - Hill Book Co., 1976, PP. 79 - 89.

16. P. Dunn, and D. A. Reay, "Heat Pipes," Pergamon Press, 1982, PP. 45 - 48.

17. M. Kuramae, "Transient Heat Transfer Characteristics of Heat Pipes," 6th International Heat Pipe Conf., Grenoble, France, May 1987.

18. W. S. Chang, "Heat Pipe Startup form the Supercritical State," Ph. D. Dissertation, Georgia Institute of technology, March 1981.

LIST OF SYMBOLS

a	condensation or evaporation coefficient
A	area
A_c	cross-section area of the vapor space
C	volumetric heat capacity
D	height of the vapor space
F	friction factor
h	enthalpy
h_{cr}	heat transfer coefficient
h_{fg}	latent heat of vaporization
$f_i(x)$	functions which describe the curvatures of the wing section
K	thermal conductivity
K_n	Knudsen number
L	total length of heat pipe
l	direction cosine
M	molecular weight
$\dot{m}$	rate of condensation or evaporation
m	number of element at the interface
n	unit outward direction
P	pressure
$\dot{Q}$	heat input rate
$\ddot{Q}$	heat input rate per unit area
R	thermal resistance
R_u	universial gas constant
S	chordwise direction

t	time
T	temperature
$T_\circ$	initial temperature
U	x - component of velocity
V	y - component of velocity
X	coordinate direction
Y	coordinate direction
W	width of the vapor space

Greek symbols

α	momentum factor
β	energy factor
γ	ratio of specific heat
ε	emissivity
λ	length of mean free path
μ	dynamic viscosity
ρ	density
σ	Stefan-Boltzmann constant
ψ	angle used to identify chordwise
τ	shear stress

Subscripts

1	heat pipe shell
2	capillary structure
c	condenser
cr	convection
e	evaporator
f	liquid state

i	index
o	liquid-vapor interface
r	radiation
x	x direction
y	y direction
v	vapor state

Superscripts

*	transition from free molecular flow to continuum